Journal of Alloys and Compounds 772 (2019) 735–739

Contents lists available at ScienceDirect

Journal of Alloys and Compounds

journal homepage: http://www.elsevier.com/locate/jalcom

Experimental determination of liquidus projection in the Cr rich region of the Cr-Si-B system

V.M. Chad [a], N. Chaia [b, *], T.F. Villela [c], C.A. Nunes [b], G.C. Coelho [b]

[a] Instituto de Ciências Agrárias e Tecnológicas, Universidade Federal de Mato Grosso, Rodovia Rondonópolis-Guiratinga, km 06 (MT-270) - Sagrada Família, 78.735-901, Rondonópolis, Mato Grosso, Brazil
[b] Escola de Engenharia de Lorena, Universidade de São Paulo, Pólo Urbo-Industrial Gleba AI-6, 12602-810, Lorena, São Paulo, Brazil
[c] Escola de Engenharia Industrial Metalúrgica de Volta Redonda, Universidade Federal Fluminense, Volta Redonda, Rio de Janeiro, Brazil

ARTICLE INFO

Article history:
Received 4 April 2018
Received in revised form
10 August 2018
Accepted 12 September 2018
Available online 13 September 2018

Keywords:
Phase diagram
Cr-Si-B
Casting
Liquidus projection

ABSTRACT

In this work, the Cr-rich region of the Cr-Si-B system have been experimentally investigated on arc-melted alloys in order to build the liquidus projection. The determination of the liquid-solid equilibria has been based on microstructural characterization of the as-cast alloys by using scanning electron microscopy and X-rays diffraction. Six primary solidification regions associated to the alloys were identified: Cr_{ss}, Cr_2B, Cr_3Si, Cr_5B_3, Cr_5Si_3 and CrB. Two ternary type II invariant reactions were identified: $Liq+Cr_5B_3 \leftrightarrow Cr_3Si+Cr_2B$ and $Liq+CrB \leftrightarrow Cr_5B_3+Cr_5Si_3$ designated by II_1 and II_2, respectively. Two ternary eutectics I_1 and I_2 corresponding, respectively, to $Liq \leftrightarrow Cr_{ss}+Cr_2B+Cr_3Si$ and $Liq \leftrightarrow Cr_5Si_3+Cr_5B_3+Cr_3Si$ were also proposed.

1. Introduction

The design of new high temperature structural materials with properties exceeding those of Ni-based superalloys is a very complex task. The challenge consists of developing materials that may satisfy strict specifications by combining stable mechanical properties and high corrosion resistance at high temperatures. Multiphase alloys consisting of metal-intermetallic composites based on refractory metals, especially those based on Mo and Nb, are considered the most promising materials for applications in the future thermal turbomachines [1,2]. The main drawback of these alloys is their poor oxidation resistance, especially at intermediate temperatures ~500–800 °C (pesting) for which the use of protective coatings is required [3,4]. A famous composition of coatings is that proposed by Sama and Priceman (commercially designated by R512E) based on Fe, Cr and Si, which is the industrial standard nowadays for Nb based alloys, elaborated using fused slurry technique or pack cementation [5,6]. Addition of boron to the coating was considered to be particularly interesting for improving oxidation resistance of silicides coatings by forming a self-healing protective layer of borosilicate at elevated temperatures [7,8]. It is worth to note that the knowledge of phase diagrams associated to the coatings-substrate system plays a pivotal role in the design and development of new coating compositions. The ternary Cr-Si-B is one of the key systems for coatings based on the Fe-Cr-Si-B system. Thus, the present work aims at the experimental investigation of the liquidus projection in the Cr-rich corner of the Cr-Si-B system (up to 60 at. % of Cr).

The liquid-solid phase equilibria in the binaries Cr-Si and Cr-B were widely investigated by several authors and are considered well established [9–15]. The invariant reactions involving the liquid phase from the binary edges Cr-Si and Cr-B from their Cr-rich portion up to 60 at. % of Cr are presented in Table 1. For the ternary system Cr-Si-B the only experimental data available in the literature refers to the partial isothermal section at 1300 °C reported by Nowotny et al. [16] which is presented in Fig. 1. The authors reported in their work: i) the existence of a ternary phase identified as $D8_8$ with a stoichiometric composition of Cr_5Si_3B, ii) important solubilities of Si in Cr_5B_3 (8 at. %) and of B in Cr_5Si_3 (4 at. %) and iii) negligible solubilities of Si in Cr_4B and Cr_2B as well as of B in Cr_3Si. To the best of our knowledge, no data related to the liquidus projection of this system has been reported in the literature.

---

* Corresponding author.
E-mail addresses: vanessamotta@ufmt.br (V.M. Chad), nabil.chaia@usp.br (N. Chaia), tales@metal.eeimvr.uff.br (T.F. Villela), cnunes@demar.eel.usp.br (C.A. Nunes), coelho@demar.eel.usp.br (G.C. Coelho).

https://doi.org/10.1016/j.jallcom.2018.09.139

Table 1
Invariant reactions on Cr rich portions (100–50 at. % of Cr) of the Cr-Si and Cr-B binary systems [19].

Invariant reaction	Compositions (at.% of Cr)			Temperature (°C)	Type of reaction
L ↔ Cr		100		1863	melting
L ↔ $Cr_3Si + (Cr_{ss})$	85	77.5	90.5	1705	Eutectic
L ↔ Cr_3Si		75		1770	Congruent
L ↔ $Cr_5Si_3 + Cr_3Si$	65	64	73.6	1660	Eutectic
L ↔ Cr_5Si_3		62.5		1680	Congruent
βCr_5Si_3 ↔ αCr_5Si_3		64–59		1505	Polymorphic transformation
L + Cr_5Si_3 ↔ CrSi	49	59	50	1413	Peritectic
L ↔ $Cr_2B + (Cr_{ss})$	86.5	66.7	99	1630	Eutectic
L + Cr_5B_3 ↔ Cr_2B	69	62.5	66.7	1870	Peritectic
L + CrB ↔ Cr_5B_3	66	50	62.5	1900	Peritectic

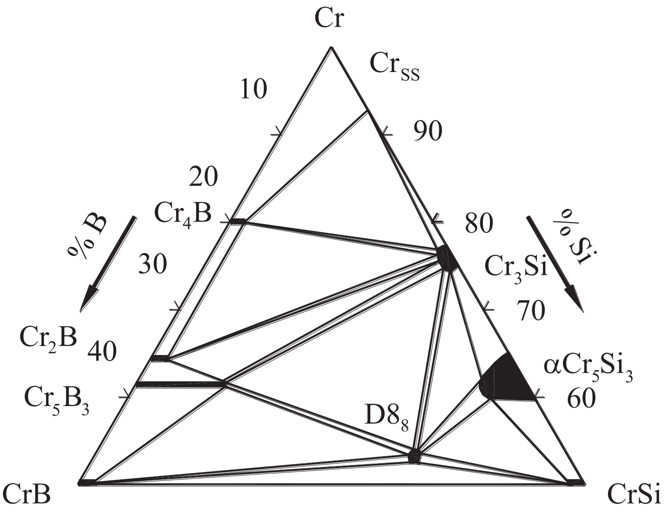

Fig. 1. Partial isothermal section at 1300 °C on the Cr rich corner of the Cr-Si-B adapted from Nowotny et al. [16].

2. Experimental procedure

The liquidus projection was experimentally determined from a set of 23 alloys using high-purity elements Cr (min. 99.95 wt %), B (min. 99.5 wt %) and Si (min. 99.998 wt %). The nominal compositions of the alloys are given in Table 2. The alloys (mass of 3 g each) were arc-melted under titanium-gettered argon atmosphere in a water-cooled copper crucible using a non-consumable tungsten electrode. The samples were melted at least four times in order to produce chemically homogeneous ingots. Projection of particles from the crucible and volatilization of elements during the melting were negligible since the maximum mass loss measured did not exceed 1 wt %.

As-cast samples were characterized by X-ray diffraction (XRD, Cu-K$_\alpha$) and scanning electron microscopy (SEM/Backscattered Electron Image mode). For the SEM analyses the samples were prepared following standard metallographic procedures: hot mounting in resin, grinding with SiC paper (#180 to #4000) and final polishing with 0.05 μm colloidal silica suspension (OP-S). The micrographs were obtained in a LEO 1450VP SEM instrument at 20 keV and 15 mm working distance. It is worth mentioning that identification of phases on the micrographs was based on XRD data and SEM/BSEI contrasts. The mean atomic number $\overline{Z} = \sum_{i=1}^{n} Z_i C_i$ (where Z_i is the atomic number and C_i is the mass fraction of the elements i) values, calculated for the different identified phases are equal to: 24, 22.47, 21.55, 22.21, 21.44 and 20.73 respectively for Cr, Cr_3Si, Cr_5Si_3, Cr_2B, Cr_5B_3 and CrB. The X-ray diffraction (XRD) characterizations were performed on powders from mechanically ground samples. The experiments were carried out using Cu–K$_\alpha$ radiation at room temperature under the following conditions:

Table 2
Nominal compositions of the investigated as cast alloys and the nature of the phases characterized by XRD.

Alloy #°	Nominal compositions (at. %)	Mass change (%)	Phases identified by XRD
1	90Cr2Si8B	0.41	$Cr_{ss} + Cr_2B$
2	87Cr6.5Si6.5B	0.35	$Cr_{ss} + Cr_2B$
3	84Cr13Si3B	0.34	$Cr_{ss} + Cr_2B + Cr_3Si$
4	80Cr10Si10B	0.41	$Cr_{ss} + Cr_2B + Cr_3Si$
5	80Cr3Si17B	0.41	$Cr_{ss} + Cr_2B$
6	78Cr9Si13B	0.34	$Cr_{ss} + Cr_2B + Cr_3Si$
7	75Cr6Si19B	0.83	$Cr_{ss} + Cr_2B + Cr_3Si$
8	72Cr3Si25B	0.51	$Cr_{ss} + Cr_2B + Cr_3Si$
9	75Cr12Si13B	0.23	$Cr_{ss} + Cr_2B + Cr_3Si$
10	78Cr13Si9B	1.30	$Cr_{ss} + Cr_2B + Cr_3Si$
11	77Cr20Si3B	1.27	$Cr_{ss} + Cr_3Si$
12	75Cr21Si4B	0.75	$Cr_{ss} + Cr_3Si$
13	70Cr27Si3B	0.31	$Cr_5Si_3 + Cr_3Si$
14	70Cr20Si10B	0.28	$Cr_5Si_3 + Cr_5B_3 + Cr_3Si$
15	70Cr10Si20B	1.20	$Cr_5B_3 + Cr_2B + Cr_3Si$
16	67Cr6Si27B	0.62	$Cr_5B_3 + Cr_2B + Cr_3Si$
17	65Cr19Si16B	0.45	$Cr_5B_3 + Cr_5Si_3 + Cr_3Si$
18	64Cr30Si6B	0.26	$Cr_5B_3 + Cr_5Si_3 + Cr_3Si$
19	60Cr30Si10B	0.09	$CrB + Cr_5Si_3$
20	62Cr26Si12B	0.29	$CrB + Cr_5B_3 + Cr_5Si_3 + Cr_3Si$
21	62Cr23Si15B	0.31	$CrB + Cr_5B_3 + Cr_5Si_3 + Cr_3Si$
22	63Cr21Si16B	2.29	$CrB + Cr_5B_3 + Cr_5Si_3 + Cr_3Si$
23	64Cr14Si22B	1.25	$CrB + Cr_5B_3 + Cr_5Si_3 + Cr_3Si$